ESC European Society of Cardiology

Cardiovascular Research (2019) **115**, 752–764
doi:10.1093/cvr/cvy257

Regional diastolic dysfunction in post-infarction heart failure: role of local mechanical load and SERCA expression

Åsmund T. Røe[1,2]*, Marianne Ruud[1,2†], Emil K. Espe[1,2†], Ornella Manfra[1,2], Stefano Longobardi[3], Jan M. Aronsen[1,4], Einar Sjaastad Nordén[1,2,4], Trygve Husebye[5], Terje R.S. Kolstad[1,2], Alessandro Cataliotti[1,2], Geir Christensen[1,2], Ole M. Sejersted[1], Steven A. Niederer[3], Geir Øystein Andersen[5], Ivar Sjaastad[1,2], and William E. Louch[1,2]

[1]Institute for Experimental Medical Research, Oslo University Hospital, University of Oslo, Kirkeveien 166, 0450 Oslo, Norway; [2]KG Jebsen Center for Cardiac Research, University of Oslo, Oslo, Norway; [3]Biomedical Engineering Department, The Rayne Institute, King's College, London, London, UK; [4]Bjørknes College, Oslo, Norway; and [5]Department of Cardiology, Oslo University Hospital Ullevål, Oslo, Norway

Received 11 September 2018; revised 8 October 2018; editorial decision 11 October 2018; accepted 22 October 2018; online publish-ahead-of-print 23 October 2018

Time for primary review: 22 days

Aims Regional heterogeneities in contraction contribute to heart failure with reduced ejection fraction (HFrEF). We aimed to determine whether regional changes in myocardial relaxation similarly contribute to diastolic dysfunction in post-infarction HFrEF, and to elucidate the underlying mechanisms.

Methods and results Using the magnetic resonance imaging phase-contrast technique, we examined local diastolic function in a rat model of post-infarction HFrEF. In comparison with sham-operated animals, post-infarction HFrEF rats exhibited reduced diastolic strain rate adjacent to the scar, but not in remote regions of the myocardium. Removal of Ca^{2+} within cardiomyocytes governs relaxation, and we indeed found that Ca^{2+} transients declined more slowly in cells isolated from the adjacent region. Resting Ca^{2+} levels in adjacent zone myocytes were also markedly elevated at high pacing rates. Impaired Ca^{2+} removal was attributed to a reduced rate of Ca^{2+} sequestration into the sarcoplasmic reticulum (SR), due to decreased local expression of the SR Ca^{2+} ATPase (SERCA). Wall stress was elevated in the adjacent region. Using *ex vivo* experiments with loaded papillary muscles, we demonstrated that high mechanical stress is directly linked to SERCA down-regulation and slowing of relaxation. Finally, we confirmed that regional diastolic dysfunction is also present in human HFrEF patients. Using echocardiographic speckle-tracking of patients enrolled in the LEAF trial, we found that in comparison with controls, post-infarction HFrEF subjects exhibited reduced diastolic train rate adjacent to the scar, but not in remote regions of the myocardium.

Conclusion Our data indicate that relaxation varies across the heart in post-infarction HFrEF. Regional diastolic dysfunction in this condition is linked to elevated wall stress adjacent to the infarction, resulting in down-regulation of SERCA, disrupted diastolic Ca^{2+} handling, and local slowing of relaxation.

Keywords Heart failure • Diastolic dysfunction • Cardiomyocyte calcium cycling • Post-infarction remodelling • Wall stress

1. Introduction

Heart failure may result from either inadequate ejection of blood during systole (systolic dysfunction) or impaired filling during diastole (diastolic dysfunction). Many heart failure patients exhibit significant systolic dysfunction and are classified as having heart failure with reduced ejection fraction (HFrEF).[1] An important cause of systolic dysfunction in HFrEF is regional heterogeneity in contraction across the left ventricle, and in

* Corresponding author. Tel: +47 23 01 6800; fax: +47 23 01 6799, E-mail: a.t.roe@medisin.uio.no

† These authors contributed equally to this manuscript.

patients with a myocardial infarction contractile dysfunction is particularly prominent adjacent to the scar.[2] While several mechanisms may promote remodelling near the infarct, including neurohumoral and paracrine signalling, we recently demonstrated that elevated wall stress in this region directly triggers disruption of cardiomyocyte t-tubules, Ca^{2+} homoeostasis, and local contractile function.[3]

In addition to systolic impairments, HFrEF patients also frequently exhibit left ventricular diastolic dysfunction.[4,5] Importantly, abnormal ventricular filling has been shown to be an independent predictor of mortality in HFrEF,[6] suggesting that diastolic dysfunction is a key pathophysiological mediator of disease progression. As with systolic dysfunction, diastolic impairment in HFrEF has been traced to altered cardiomyocyte Ca^{2+} homoeostasis. Specifically, reduced expression of the sarcoplasmic reticulum (SR) Ca^{2+} ATPase 2 (SERCA) and, in some cases, decreased activity of the Na^{+}/Ca^{2+} exchanger (NCX), lead to slowed removal of cytosolic Ca^{2+} and slowed, incomplete relaxation.[7–9] However, while local differences in systolic function are established to be a central feature of HFrEF, it is unknown whether global diastolic dysfunction results from regional changes in myocardial relaxation. We presently investigated diastolic function across the hearts of post-infarction HFrEF rats and patients, and hypothesized that relaxation is particularly impaired adjacent to the scar due to wall stress-induced disruption of diastolic Ca^{2+} handling.

2. Methods

An expanded methods section is available in the Supplementary material online.

2.1 Animal model

All animal experiments were approved by the Norwegian Animal Research Authority and performed in accordance with the Norwegian Animal Welfare Act and NIH Guidelines (NIH publication No. 85-23, revised 2011). Myocardial infarction was induced by coronary artery ligation in anaesthetized male Wistar rats (endotracheal ventilation with a mixture of 2.5% isoflurane, 97.5% O_2).[3] Sham-operated rats served as controls. Post-infarction rats that had progressed into heart failure 6 weeks after surgery were selected based on established echocardiographic criteria (large infarct size and left atrial diameter >5 mm).[10] Mean infarct size was 40.5% of the left ventricular wall (standard deviation 6.6%, range 27.3–51.5%). Other animal characteristics are presented in *Table 1*. The current work employed an expanded cohort of sham and HFrEF animals compared with the work previously published by Frisk *et al.*[3]

2.2 *In vivo* characterization of HFrEF and sham rats

Rats were characterized *in vivo* by echocardiography and magnetic resonance imaging (MRI). For echocardiography, anaesthesia was induced by O_2 and isoflurane (4.0%), and maintained in freely breathing animals using O_2 and isoflurane (1.75%). Doppler inflow recordings were used to calculate left ventricular peak trans-mitral flow (E) and peak trans-mitral deceleration rate.

MRI was performed on a 9.4T preclinical MRI system with hardware dedicated for rat cardiac imaging. Anaesthesia was induced in a chamber with O_2/4.0% isoflurane, and adjusted during examination using O_2/1.5–2.0% isoflurane to maintain stable anaesthesia. Respiration, electrocardiogram, and body temperature were continuously monitored, and the latter maintained at 37°C using heated air. As described in detail in the Supplementary material online, three short-axis slices (basal, mid-ventricular, and apical) were acquired in each animal using phase-contrast MRI.[11] The myocardium was segmented semiautomatically[12] and the viable myocardium divided into three equally sized regions adjacent, medial, and remote to the infarct (*Figure 1A*). In each region, circumferential strain and strain rate were calculated as previously described.[13] MRI-based estimates of local curvature and wall thickness and catheter-based measurements of intraventricular pressure enabled calculation of wall stress (expressed as an integration of diastolic and systolic values).[3] Hearts were then excised from sedated animals, immediately immersed in ice-cold saline, weighed, and used for further experiments.

Table 1 Animal characteristics

	Sham	HFrEF
Post-mortem (n = 14, 21)		
Heart to body weight ratio (mg/g)	3.10 ± 0.13	5.51 ± 1.21*
Lung to body weight ratio (mg/g)	3.37 ± 0.17	10.55 ± 0.53*
Echocardiography (n = 13, 21)		
Heart rate (min^{-1})	409.8 ± 9.7	362.1 ± 7.5*
Peak trans-mitral flow (E) (mm/s)	894.7 ± 16.1	1085.7 ± 54.8*
Peak trans-mitral deceleration rate (cm/s^2)	2968 ± 277	5438 ± 600*
MRI (n = 14, 22)		
Ejection fraction (%)	69.6 ± 1.53	28.3 ± 8.7*
End-diastolic volume (μL)	467.0 ± 13.9	1052 ± 33*
End-systolic volume (μL)	142.6 ± 8.6	755.6 ± 26.3*
Left ventricular mass (g)	0.70 ± 0.02	0.77 ± 0.02*
Left ventricular catheterization (n= 14, 22)		
End-diastolic pressure (mmHg)	2.14 ± 0.27	26.5 ± 0.8*
dP/dt_{min} (mmHg/ms)	30 792 ± 1524	18 595 ± 551*

Rats which developed HFrEF 6 weeks following myocardial infarction were functionally compared with sham-operated controls.
*$P < 0.05$ vs. sham measured by Student's t-test.

2.3 Cardiomyocyte Ca^{2+} imaging

For single cell experiments, left ventricular cardiomyocytes were isolated as described previously.[14] Briefly, excised hearts were perfused in a Langendorff setup with an isolation buffer containing collagenase. The remote, medial, and adjacent regions were then separated and individual cardiomyocytes isolated by a secondary digestion and agitation.[14]

Whole-cell, wide-field Ca^{2+} transients were recorded in cardiomyocytes pre-incubated with 10 μmol/L fluo 4-AM.[14] Cells were plated on the stage of an inverted microscope and superfused with a Hepes Tyrode's solution containing 1.8 mmol/L $CaCl_2$ at 37°C, and field-stimulated at a range of frequencies (0.5, 1, 2, 4, and 6 Hz). By rapidly applying 10 mmol/L caffeine, we used mono-exponential fits of the decay of the elicited transient to define the rate constant of Ca^{2+} extrusion ($1/\tau_{caff}$). The NCX contribution to Ca^{2+} extrusion was defined as the change in rate constant resulting from application of 5 mmol/L Ni^{2+}, an NCX antagonist, while remaining Ca^{2+} flux was attributed to slow extrusion pathways. The rate of SERCA-dependent Ca^{2+} reuptake was calculated by subtracting the extrusion rate constant from the rate constant of Ca^{2+} decay measured during 1 Hz Ca^{2+} transients ($1/\tau_{1Hz} - 1/\tau_{caff}$).[14]

Diastolic $[Ca^{2+}]_i$ was determined in cardiomyocytes loaded with 5 μM fura-2 AM, and these values were employed to calibrate fluo-4 recordings as described previously.[14–16]

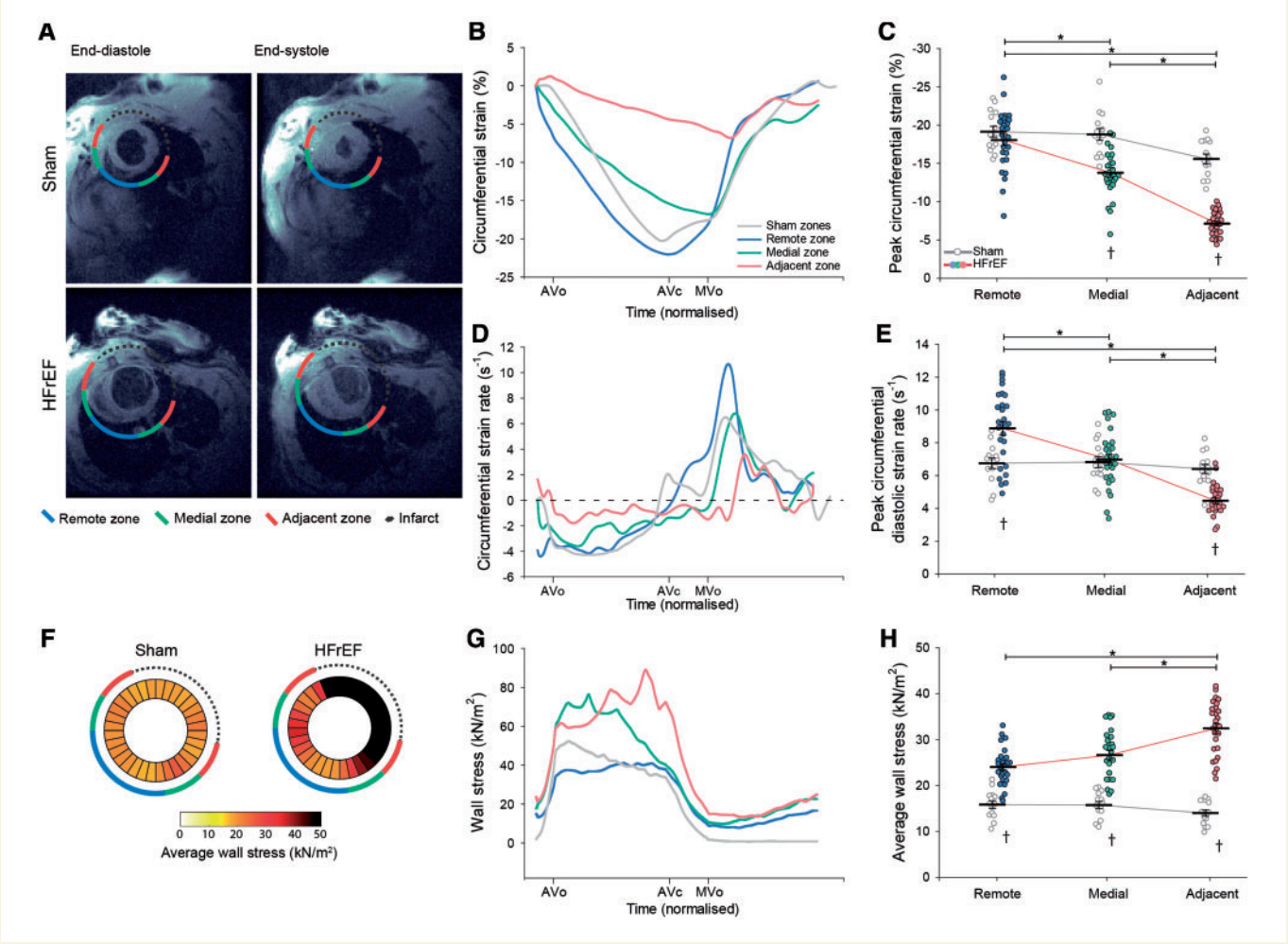

Figure 1 Slowing of relaxation and elevated wall stress in the adjacent region of HFrEF rats. MRI images illustrate the division of HFrEF rat hearts into three regions (adjacent, medial, and remote) according to their proximity to the infarction (*A*). Comparison was made to equivalent regions in sham-operated controls. Representative recordings (*B*) and mean data (*C*) revealed lower peak circumferential systolic strain adjacent to the infarct in HFrEF. The rate of relaxation was dyssynchronous across the failing heart, as indicated by measurements of circumferential strain rate (*D*). Specifically, peak diastolic strain rate was only reduced in the adjacent region of HFrEF hearts, and was increased in the remote region (*E*). Wall stress was calculated across sham and HFrEF hearts based on intraventricular pressure measurements and local ventricular geometry (see Methods section). Measurements are presented as bullseye plots (*F*) and tracings of wall stress values during the cardiac cycle (*G*). Mean data demonstrate that while integrated wall stress was high in all regions of HFrEF hearts, values were particularly elevated in the adjacent region (*H*). (n_{hearts} = 14, 29 in sham, HFrEF). *$P < 0.05$ calculated by two-way ANOVA with a *post hoc* Bonferroni *t*-test. AVc, aortic valve closure; AVo, aortic valve opening; MVo, mitral valve opening.

2.4 Modelling

Rat ventricular cardiomyocyte electrophysiology and Ca^{2+} dynamics were simulated using the model of Gattoni *et al.*,[17] to investigate the consequences of alterations in Ca^{2+} fluxes observed experimentally. The isolated effects of a 45% increase in NCX conductance or 25% reduction in SERCA conductance on the overall Ca^{2+} transient were determined by allowing the model to run to steady-state during 6 Hz stimulation.

2.5 Papillary muscle experiments

We examined the effect of mechanical stress on myocardial diastolic function in papillary muscles excised from the left ventricle and mounted in a myobath system as previously described.[3] Muscles were stretched to achieve either normal (≈4 kN/m^2) or high diastolic stress (≈15–20 kN/m^2), and electrically field-stimulated to develop isometric force during 48 h of culture (*Figure 5A*). Only muscles that developed ≥1.5 mN force were included. Muscle core ischaemia was avoided by employing a relatively slow pacing rate (0.5 Hz) and low temperature (22°C); indeed, lactate values (in mmol/kg wet weight) in normal (10.8 ± 2.7) and high stress groups (11.2 ± 3.5) were similar to values in freshly isolated muscles (7.5 ± 0.53, *P* = NS). After 48 h, muscles subjected to high diastolic stress were returned to a normal stress level (≈4 kN/m^2) and allowed to stabilise for 10 min while force was recorded. After completion of the experimental protocol, papillary muscles were snap frozen in liquid nitrogen and stored for molecular analysis.

2.6 Western blotting

Frozen tissue from rat left ventricles was homogenized and protein concentrations quantified as previously described.[3] Primary antibodies for immunoblotting were SERCA2, NCX1, phospholamban, phospholamban

Table 2 Patient characteristics

	Non-failing ($n = 12$)	HFrEF ($n = 9$)
Age (years)	64 ± 3.7	62 ± 3.7
Heart rate (min^{-1})	62 ± 2.5	77 ± 4.2*
End-diastolic volume (mL)	90 ± 12.1	143 ± 11.6*
End-systolic volume (mL)	37 ± 5.0	95 ± 9.1*
Left ventricular ejection fraction (%)	59 ± 1.4	34 ± 1.6*
E/A	1.5 ± 0.20	1.1 ± 0.17
E/e′	10.4 ± 1.0	11.9 ± 1.2
S/D	1.14 ± 0.07	1.07 ± 0.13
Diastolic blood pressure (mmHg)	78 ± 2.4	78 ± 3.1
Systolic blood pressure (mmHg)	123 ± 6.5	116 ± 4.8
Infarct size (%)	32 ± 6.0	54 ± 2.6

Participants in the LEAF trial[18] exhibiting HFrEF were compared with non-failing individuals at 6 weeks of follow-up (see Fig. 6 for inclusion criteria).
E/A, mitral valve E-wave velocity/A-wave velocity, *E/e′*, mitral valve *E* velocity/mitral annular *e′* velocity; S/D, pulmonary vein S-wave/D-wave velocity.
*$P < 0.05$ vs. control measured by Student's *t*-test.

Ser16, phospholamban Thr17, $Ca_v1.2$, and vinculin. We also used western blotting to assess MEK and ERK signalling pathways, as described in the Supplementary material online. Secondary antibodies were anti-goat IgG HRP-conjugated antibody, anti-rabbit, or anti-mouse IgG HRP-linked whole antibody.

2.7 PCR

Papillary muscle tissue was gently defrosted and mRNA extracted using an RNeasy Mini Kit (Qiagen, Hilden, Germany). qPCR was then performed to quantify SERCA2 and NCX1 gene expression, normalized to the expression of housekeeping gene Ribosomal Protein L4.

2.8 Human echocardiography

We examined local diastolic function in a selection of patients enrolled in the LEAF (LEvosimendan in Acute heart Failure following myocardial infarction) trial (NCT00324766).[18] Briefly, this study randomized patients with percutaneous coronary intervention-treated ST-elevation myocardial infarction complicated with symptomatic acute heart failure to 24 h infusion of levosimendan or placebo. The Regional Ethics Committee approved the study, and it was conducted in accordance with the principles of the Declaration of Helsinki. All patients provided written informed consent.[18] Levosimendan treatment was observed to only transiently augment cardiac function in the initial days following treatment.[18,19] We presently examined echocardiographic four-chamber apical recordings from study participants at 6 weeks of follow-up, and included those with high acoustic quality of recordings, apical infarctions, and reduced ejection fraction (<40%, *Figure 6*). The viable myocardium of the lateral and septal walls was divided into three equally sized regions (*Figure 7A*), and speckle-tracking was performed on kernels in the middle of the remote and adjacent regions (B-mode recordings; frame rate = 68 ± 2.7 frames/s). Peak early diastolic strain rate was calculated as the average of values from the septal and lateral walls. Measurements were compared with regionally matched values from patients in the same study cohort with an ejection fraction ≥50% at 6 weeks of follow-up, and who were without a visible infarction in four-chamber view (*Figures 6 and 7*). Trans-mitral and pulmonary vein velocities, left ventricular ejection fraction, and end-diastolic volume were calculated as previously described.[18] Blood pressure was measured with a brachial cuff at the same time point. Patient characteristics are presented in *Table 2*.

2.9 Statistical analysis

All results are expressed as mean values ± standard error of the mean. Statistical significance was calculated by the Student's *t*-test for unpaired data. Nested ANOVA or two-way ANOVA analysis with a *post hoc* Bonferroni *t*-test was used where appropriate, as indicated in the figure legends. Statistical significance was defined as $P < 0.05$.

3. Results

3.1 Regional diastolic dysfunction and elevation of wall stress in HFrEF rats

Regional diastolic function was investigated in an experimental rat model of HFrEF. Animals that developed heart failure 6 weeks following myocardial infarction exhibited characteristic increases in end-diastolic left ventricular pressure and diameter, and marked reduction in global systolic and diastolic function (*Table 1*). MRI-based segmentation of the viable myocardium into regions adjacent, medial, and remote to the infarction (*Figure 1A*) revealed marked differences in regional function. Peak circumferential systolic strain was most markedly reduced in the adjacent region, but equivalent to sham values in the remote region (*Figure 1B and C*). Furthermore, we observed that local diastolic dysfunction, as assessed by diastolic strain rate, also occurred only in regions adjacent to the infarction (*Figure 1D and E*). As high wall stress may be a trigger for remodelling,[3] we examined local left ventricular wall stress across HFrEF and sham hearts (wall stress = pressure × local radius/2 × wall thickness). Wall stress was increased in HFrEF hearts, and was particularly elevated adjacent to the myocardial scar tissue due to local flattening of curvature and thinning of the ventricular wall (*Figure 1F–H*).[3]

3.2 Impaired diastolic Ca^{2+} removal adjacent to the infarction

We next investigated whether variable wall stress and local slowing of relaxation in HFrEF were associated with regional differences in cardiomyocyte Ca^{2+} handling. Myocytes isolated from the three regions of HFrEF hearts and equivalent regions in sham were field-stimulated to elicit Ca^{2+} transients across a range of frequencies (*Figure 2A*). The magnitude of Ca^{2+} transients was reduced in the medial and remote region in HFrEF, but maintained in the adjacent region (*Figure 2B*). However, the declining phase of the Ca^{2+} transient was markedly slowed in the adjacent region in HFrEF compared with sham (*Figure 2C*). Furthermore, adjacent region myocytes exhibited a significant accumulation of diastolic Ca^{2+} at high pacing frequencies when time available for Ca^{2+} removal was limited (*Figure 2D*). Elevated end-diastolic Ca^{2+} limits the *extent* of cardiomyocyte relaxation, whereas reduced speed of Ca^{2+} removal slows the *rate* of relaxation[9]; both alterations are consistent with the diastolic dysfunction observed *in vivo* adjacent to the infarct. By comparison, maintained diastolic function in the remote region of HFrEF hearts was associated with preserved Ca^{2+} transient decline and significantly lower diastolic Ca^{2+} levels (*Figure 2C and D*). Diastolic Ca^{2+} handling in the medial zone was intermediate between values in the adjacent and remotes zones, mirroring observations of local *in vivo* diastolic function. For clarity of presentation, statistical analysis of the frequency response of Ca^{2+}

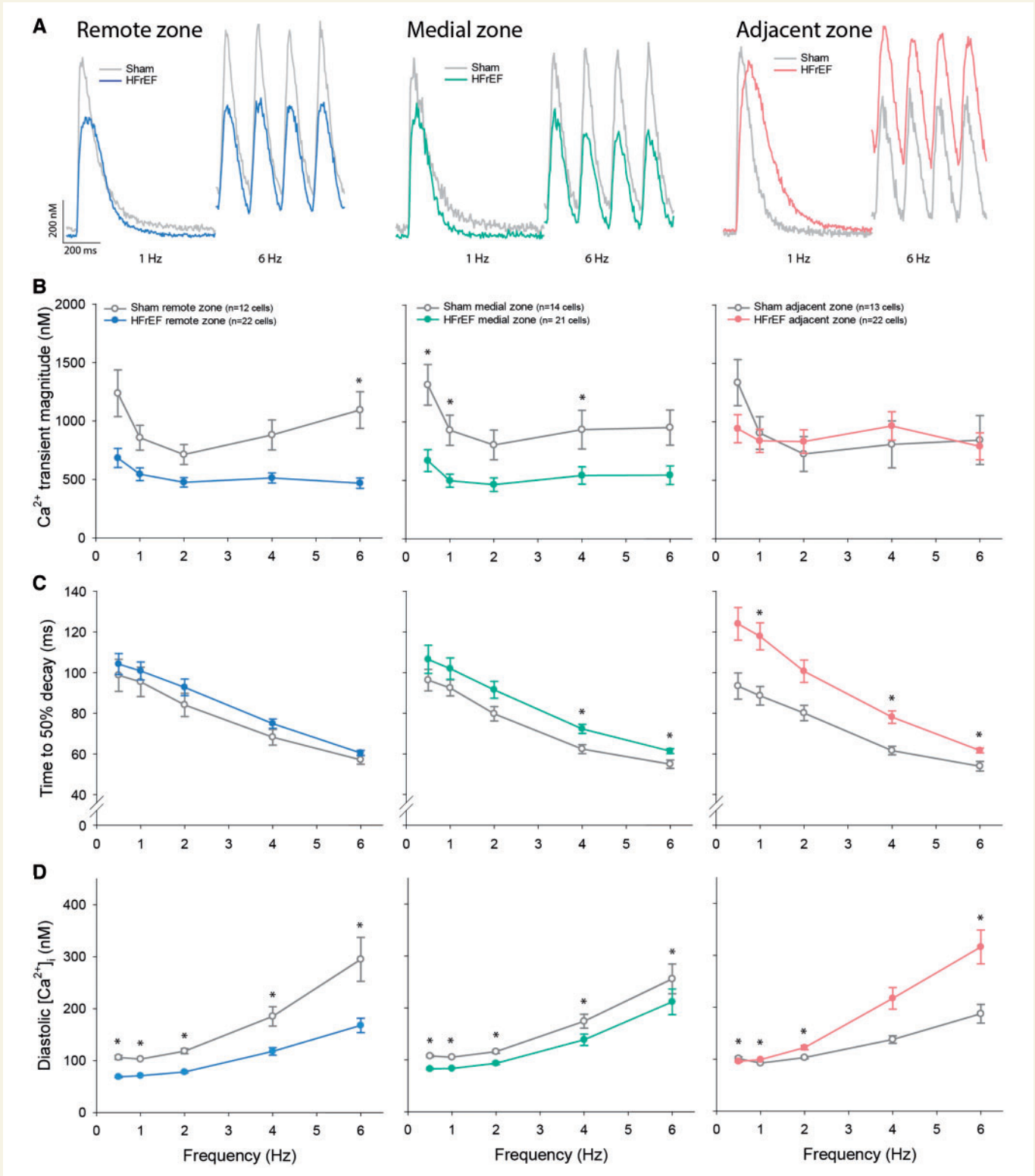

Figure 2 Impaired diastolic Ca^{2+} handling in cardiomyocytes from the adjacent region. Representative recordings of whole-cell, wide-field Ca^{2+} transients (*A*, 1 Hz and 6 Hz stimulation, fluo-4), and mean data (*B*) revealed that, relative to sham, Ca^{2+} transient magnitude was maintained in cardiomyocytes isolated from the adjacent zone of HFrEF hearts, but reduced in the medial and remote zones. However, HFrEF cells from the adjacent region exhibited significantly slower Ca^{2+} transient decay (*C*), and at high-pacing frequencies, a significant elevation of diastolic Ca^{2+} levels (*D*). (n_{hearts} = 4, 5 in sham, HFrEF). Comparisons between HFrEF regions are presented in Supplementary material online, *Figure S1*. *$P < 0.05$ vs. sham calculated with nested ANOVA.

homoeostasis across HFrEF hearts is presented in Supplementary material online, *Figure S1*.

3.3 Reduced SERCA expression and function in the adjacent region

Function of the main mediators of cytosolic Ca^{2+} removal, SERCA, and NCX, was assessed by rapid caffeine application in isolated cells (*Figure 3A*). Comparison of the decay kinetics of action potential- and caffeine-elicited Ca^{2+} transients revealed a reduced rate of SR Ca^{2+} reuptake in the adjacent region (*Figure 3C*). Protein levels of SERCA were also significantly down-regulated in this region (*Figure 4A and B*). Expression of phospholamban, the endogenous SERCA inhibitor, was unaltered (*Figure 4C*), and no change in phosphorylation status was observed at either serine-16 or threonine-17 (data not shown). Expression of other key mediators of Ca^{2+} homoeostasis was similarly unchanged (*Figure 4D–F*). Lowered expression and activity of SERCA are consistent with the slowed Ca^{2+} removal in the adjacent region, and with elevated resting Ca^{2+} levels observed at higher pacing frequencies (*Figure 2*), where SERCA activity is known to play an augmenting role in setting diastolic $[Ca^{2+}]_i$.[9]

Fits of the decays of caffeine-elicited transients were employed to assess rates of non-SERCA mediated Ca^{2+} removal, with sensitivity to 5 mmol/L Ni^{2+} used to differentiate between NCX vs. slow extrusion pathways, including the plasma membrane Ca^{2+} exchanger and mitochondrial Ca^{2+} uniporter (see Methods section). Removal of Ca^{2+} by slow pathways was similar across sham and HFrEF hearts (*Figure 3E*). However, while Ca^{2+} extrusion via NCX was also maintained in the adjacent region of HFrEF hearts, NCX activity tended to be increased in the remote zone (*Figure 3A and D*). As NCX is a key regulator of resting $[Ca^{2+}]_i$, especially at lower stimulation frequencies,[9] the graded NCX activity observed across HFrEF is consistent with observed differences in diastolic Ca^{2+} levels (*Figure 2D*).

Diastolic Ca^{2+} handling directly impacts systolic $[Ca^{2+}]_i$, as competing NCX and SERCA activities and resting Ca^{2+} levels importantly determine the extent of SR Ca^{2+} reuptake.[9] Tendencies for higher NCX activity in the remote zone and lowered diastolic $[Ca^{2+}]_i$ in the remote and medial zones were associated with decreased SR Ca^{2+} content (*Figure 3A and B*) and smaller Ca^{2+} transients (*Figure 2B*) in these regions. This finding was confirmed by mathematical modelling, which reproduced a reduction in both resting $[Ca^{2+}]_i$ and Ca^{2+} transient amplitude when NCX activity was matched to values in the remote region (*Figure 3F*). Conversely, no reduction in SR Ca^{2+} content or release (*Figure 3B and 2B*) was observed in the adjacent region, despite down-regulation of SERCA in this region. However, mathematical simulations verified that reducing SERCA activity by 25% while maintaining NCX activity only modestly affected Ca^{2+} transient amplitude, but slowed Ca^{2+} transient decline and elevated diastolic $[Ca^{2+}]_i$ (*Figure 3F*), paralleling findings in adjacent zone myocytes.

3.4 High mechanical stress down-regulates SERCA and slows relaxation *ex vivo*

In HFrEF, high *in vivo* wall stress adjacent to the infarction (*Figure 1H*) coincided with down-regulation of SERCA, disrupted cardiomyocyte Ca^{2+} handling, and impaired myocardial relaxation. To investigate the causality of these associations, we stretched explanted rat left ventricular papillary muscles to reproduce the elevated wall stress values observed *in vivo* in the adjacent region, and compared with muscles exposed to normal load (*Figure 5A*). Forty-eight hours of exposure to high load conditions triggered a marked reduction in SERCA gene expression (*Figure 5B*), and slowing of force decline during isometric electrical stimulation (*Figure 5C and D*). These observations suggest that high wall stress adjacent to the myocardial infarction directly promotes local diastolic dysfunction by signalling reduced SERCA expression and impaired removal of cytosolic Ca^{2+}. Interestingly, *Figure 5C* also demonstrates a slowing of tension development in the high stress group, consistent with stress-induced disruption of t-tubule structure and systolic function described in our previous work.[3]

3.5 Regional diastolic dysfunction in patients with post-infarction HFrEF

To investigate whether regional diastolic dysfunction is also a feature of human post-infarction HFrEF, we examined cardiac function in patients enrolled in the LEAF trial[18] that presented with reduced ejection fraction (HFrEF) 6 weeks following a myocardial infarction (*Figure 6*, *Table 2*). Compared with controls, global systolic function was reduced in HFrEF, and speckle-tracking revealed marked differences in local function (*Figure 7*). Specifically, in agreement with previous work,[2,3] we observed reduced contraction magnitude (peak systolic longitudinal strain) adjacent to the infarction (*Figure 7B*). Although less markedly altered, strain values were also somewhat reduced in the remote region of HFrEF patients, which may reflect an expected rise in filling pressures and a previously established load-dependence of strain measurements.[20] In line with our observations made in the rat model, we observed that local diastolic function varied across the failing human heart. Peak strain rate measurements revealed slowed relaxation adjacent to the infarct, but not at remote sites (*Figure 7C and D*). This spatially dyssynchronous pattern of relaxation in HFrEF patients is expected to impair early ventricular filling,[21] and indicates that measurements of local diastolic myocardial function detect diastolic abnormalities not evident from global parameters (*Table 2*).

4. Discussion

While the pathophysiology of HFrEF has traditionally been attributed to weakening of contraction, impaired left ventricular filling is highly prevalent. The present study has provided new insight into the underlying mechanisms. We observed that in a rat model of post-infarction HFrEF, regional diastolic function varied significantly across the left ventricle with slowing of relaxation adjacent to the infarction scar. Local impairment of relaxation was associated with reduction in SERCA expression and activity, and impaired diastolic Ca^{2+} removal in cardiomyocytes. *Ex vivo* experiments demonstrated that elevated wall stress, as present in the adjacent region, directly triggers reduction in SERCA expression and diastolic dysfunction. Finally, we confirmed that human patients with post-infarction HFrEF also exhibit a similar pattern of regional diastolic dysfunction. These findings reveal a novel mechanistic link between altered mechanical load, active (Ca^{2+}-dependent) myocardial stiffness, and regional variation in ventricular relaxation in HFrEF.

4.1 Regional diastolic dysfunction in post-infarction HFrEF

It is well established that global systolic and diastolic ventricular performance are depressed in HFrEF, as indicated by functional parameters such as ejection fraction and transmitral filling patterns.[4,5] However, mechanical function at the global level is in essence dependent on regional myocardial function. Indeed, global systolic dysfunction in HFrEF has

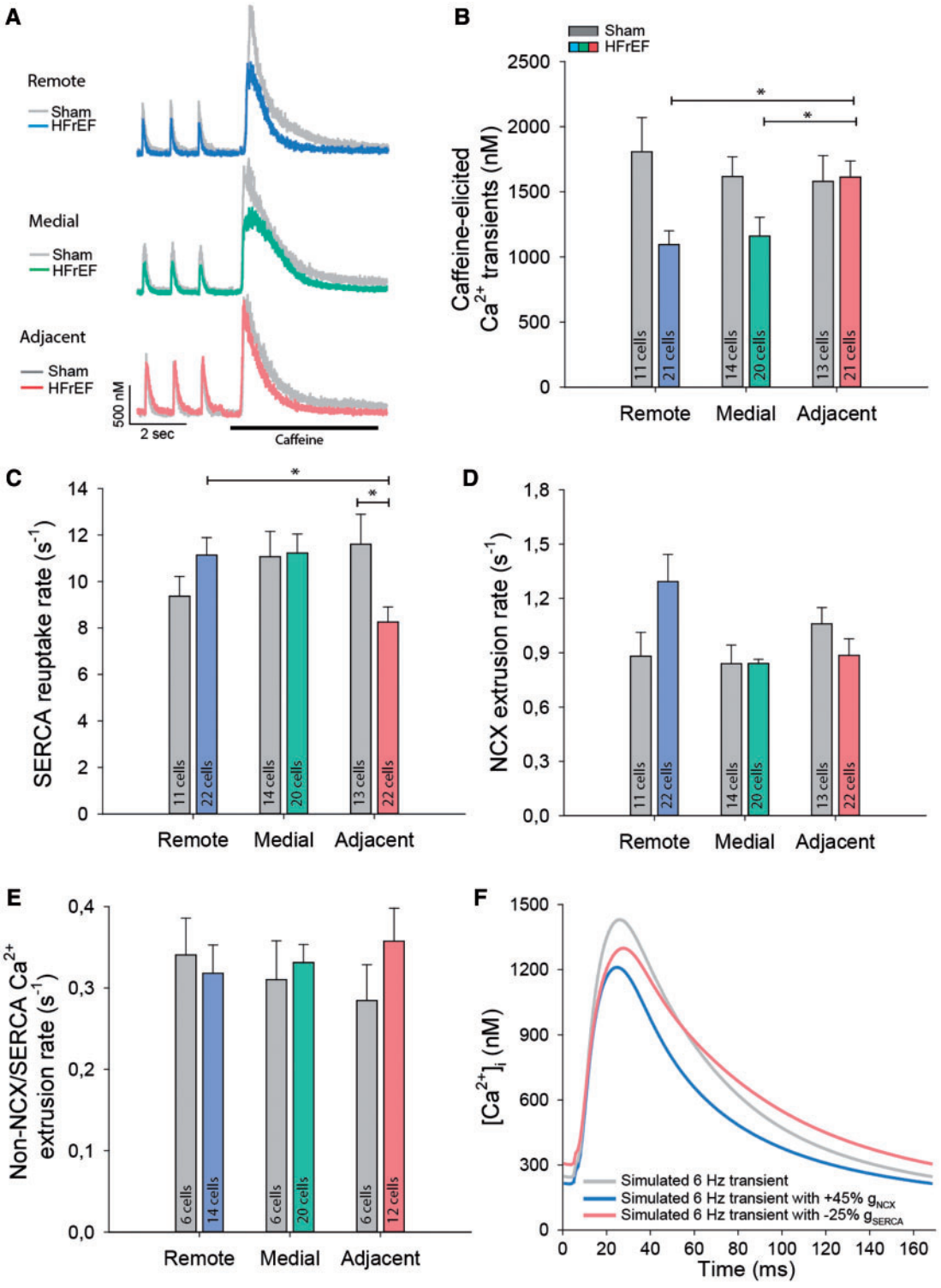

Figure 3 Reduced SERCA activity in the adjacent region. Representative recordings of Ca^{2+} transients are illustrated for cardiomyocytes during 1 Hz pacing, followed by rapid application of 10 mmol/L caffeine (*A*). The magnitude of caffeine-elicited Ca^{2+} release, an indicator of SR Ca^{2+} content, tended to be lower in the medial and distal regions (*B*). Fits of the declining phases of 1 Hz and caffeine transients revealed slowed SR Ca^{2+} reuptake in HFrEF cardiomyocytes from the adjacent region (*C*), while the rate of NCX Ca^{2+} extrusion tended to be higher in the remote zone (*D*) (n_{hearts} = 4, 5 in sham, HFrEF). (*E*) Caffeine transients recorded in the presence of 5 mmol/L Ni^{2+} revealed no alterations in Ca^{2+} fluxes via slow extrusion pathways (n_{hearts} = 2, 3 in sham, HFrEF). (*F*) Simulations of Ca^{2+} transients at physiological frequency (6 Hz) demonstrate the consequences of enhancing NCX activity (blue), as observed in myocytes from the distal zone, or reducing SERCA activity (red), as observed in the adjacent zone. *$P < 0.05$, calculated by nested ANOVA.

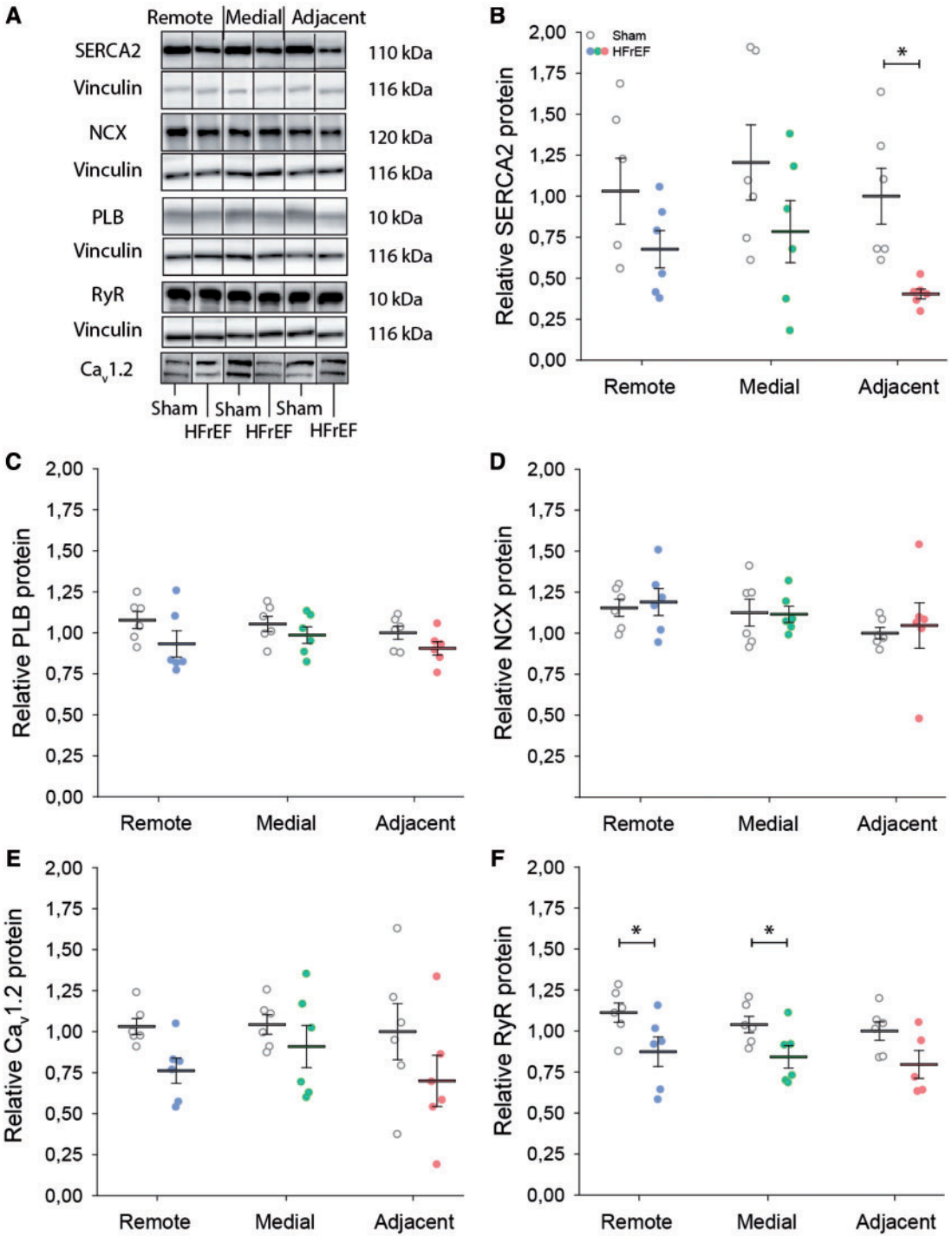

Figure 4 Lower SERCA2 expression in the adjacent region. Consistent with impaired SERCA function in the adjacent region, representative immunoblots (*A*, vinculin as loading control), and mean data (*B*) show that SERCA2 expression was significantly reduced in the adjacent region. By contrast, expression of phospholamban (PLB, *C*), NCX (*D*), the L-type Ca^{2+} channel ($Ca_v1.2$, *E*), and the ryanodine receptor (RyR, *F*) were not markedly altered across HFrEF and sham hearts. Complete blots are presented in Supplementary material online, *Figure S4* (n_{hearts} = 6, 6 in sham, HFrEF). *$P < 0.05$, calculated by two-way ANOVA with a *post hoc* Bonferroni *t*-test.

been previously linked with differences in the regional timing and magnitude of contraction across the ventricle.[2] In contrast, regional diastolic function has not been widely examined and, to the best of our knowledge, the present study represents the first description of local diastolic impairment in post-infarction HFrEF. While homogenous relaxation across the left ventricle normally ensures a rapid fall in intraventricular pressure during early diastole, we propose that regional disparities in relaxation critically contribute to global diastolic dysfunction in HFrEF. This

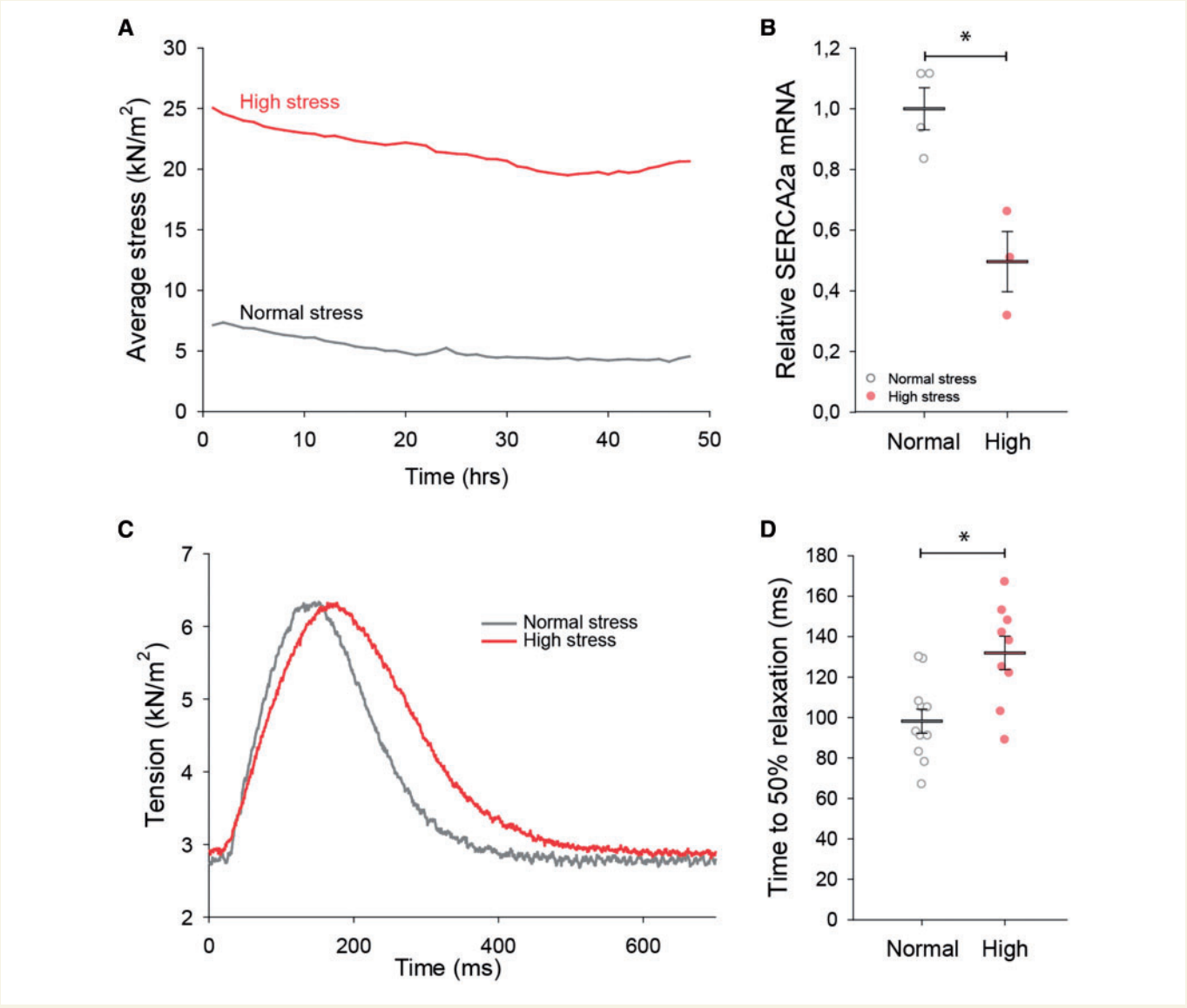

Figure 5 High mechanical stress down-regulates SERCA2 and slows relaxation in *ex vivo* myocardial tissue. Excised rat papillary muscles were stretched to reproduce high wall stress values comparable to those in the adjacent region of HFrEF hearts, and maintained during 48 h of culture. Comparison was made with muscles subjected to low wall stress conditions approximating those present in the normal heart. Average tension during the protocol is illustrated in *A* for representative muscles. High stress triggered a significant down-regulation of SERCA2 mRNA (*B*) ($n_{muscles}$ = 4 in low group, 3 in high). Returning high stress muscles to normal levels at the completion of the protocol revealed that SERCA2 down-regulation was associated with marked slowing of force decline (representative recordings in *C*; mean data in *D*) ($n_{muscles}$ = 11, 9 in low, high). *P < 0.05 vs. low stress calculated with Student's *t*-test.

notion is supported by previous work examining acute ischaemia, where slowing of relaxation in ischaemic regions was observed to decrease the mitral-to-apical pressure gradient, and disrupt the normal pattern of ventricular filling.[21] Similarly, our present observations in HFrEF rats showed depression of global diastole with elevated end-diastolic pressures (*Table 1*), but impairment of local diastolic function only adjacent to the infarction (*Figure 1E*). We similarly observed slowed relaxation only adjacent to the infarction of HFrEF patients. Of note, these measurements were compared with patients recovering from acute heart failure, i.e. not healthy individuals, which may explain why global diastolic function was not significantly different between the cohorts. We have presented only longitudinal strain and strain rate measurements in these patients since the adjacent region was often not included in short axis sections, making circumferential strain difficult to calculate. Radial strain, on the other hand, less validly reflects myocardial function since the myofibres are not arranged in this orientation.

4.2 Role of SERCA down-regulation

Our investigations in the HFrEF rat model suggest a key role of reduced SERCA expression in promoting diastolic dysfunction in the adjacent region. While other factors such as the sensitivity of the myofilaments to Ca^{2+} also affect cellular relaxation, our findings support previous work linking SERCA down-regulation and global diastolic dysfunction in human HFrEF.[8] Furthermore, knock-out of SERCA in mice significantly slows Ca^{2+} uptake and impairs diastolic function,[22] while restoration of SERCA expression in heart failure improves relaxation.[23] Thus, regional slowing of relaxation in post-infarction HFrEF may be a marker of reduced SERCA expression.

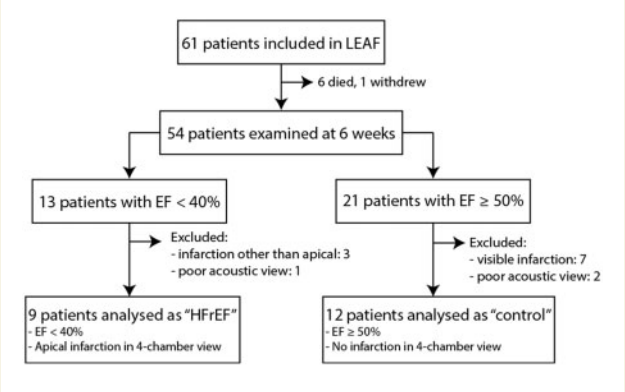

Figure 6 Selection of LEAF trial[18] participants. HFrEF patients were compared with non-failing 'control' individuals (EF ≥50%) who were without a detectable myocardial infarction at 6 weeks of follow-up.

Our data indicate that there is a complex balance of SERCA and NCX activity across HFrEF hearts which critically determines local diastolic function. We observed that SERCA loss adjacent to the infarction was not accompanied by altered NCX expression (*Figure 4D*), which appears to parallel previous whole-heart observations in human HFrEF patients with diastolic dysfunction.[7] PCR data from papillary muscles subjected to high wall stress also did not reveal significant changes in NCX at the transcriptional level, although a tendency towards down-regulation was observed (relative mRNA expression = 1.0/0.52 in low-stress/high stress). As we have previously observed marked t-tubule reorganization in the adjacent zone,[3] it may be speculated that resulting displacement of NCX from sites of Ca^{2+} release contributes to the tendency for somewhat slower NCX-mediated Ca^{2+} release and diastolic dysfunction in this region (*Figure 3D*). By contrast, HFrEF patients with *preserved* diastolic function are reported to exhibit maintained or even increased NCX levels, with the latter proposed to compensate for reduced SERCA-mediated Ca^{2+} removal.[7] Interestingly, we did presently observe a strong tendency towards increased NCX activity in the remote region, which was linked to reduced resting Ca^{2+} levels both experimentally (*Figure 2D*) and via mathematical modelling (*Figure 3F*). We believe that this represents a compensatory response of the remote myocardium to lower active resting tension. Indeed, local acceleration of re-lengthening in the remote zone was observed *in vivo*. The mechanisms underlying NCX augmentation are presently unclear, as no change in NCX protein levels was observed. However, other factors not presently investigated such as intracellular sodium homoeostasis, transmembrane potential, and the regulatory protein phospholemman are also important determinants of NCX activity.[24] Of note, while SERCA and NCX activities were observed to vary considerably across HFrEF hearts, we did not observe alterations in slow Ca^{2+} extrusion pathways, which remain present when SERCA and NCX function are blocked (caffeine and Ni^{2+} treatment, respectively, *Figure 3E*). Thus, although for instance mitochondrial structure and function are suggested to be disrupted in HFrEF,[25] we do not expect that changes in function of the mitochondrial Ca^{2+} uniporter, or plasmalemmal Ca^{2+} ATPase, are important contributors to differences in local diastolic function in HFrEF.

It is important to note that strain rate reflects not only active, Ca^{2+}-dependent myocardial relaxation, but also early diastolic load (i.e. filling pressure) and restoring forces.[20] Lengthening load was increased in the adjacent region, as evidenced by elevated diastolic wall stress, which is expected to promote *faster* re-lengthening in opposition to the effects of slowed Ca^{2+} removal. Restoring force on the other hand, is difficult to determine due to its opposing and simultaneous action with active cross-bridge tension. In general, however, restoring forces are set by the viscoelastic properties of the myocardium and the degree of systolic strain. Indeed, reductions in systolic strain as observed adjacent to the infarct may contribute to decreases in diastolic re-lengthening in this region. Likewise, diastolic dysfunction may be promoted by collagen accumulation which is reported to be particularly prominent adjacent to an infarction.[26,27] Ventricular sections from HFrEF did indeed show marked fibrosis in the adjacent region (Supplementary material online, *Figure S6*), in agreement with previous work.[26,27] Tethering to the immobile infarct may also act to reduce strain and strain rate in the adjacent region, although strain measurements based on speckle-tracking are less influenced by tethering effects than Doppler tissue imaging.[28] Furthermore, no correlation was observed between infarct size and diastolic strain rate (Supplementary material online, *Figure S7*). Nevertheless, while we believe that the diastolic deficit in the adjacent region is consistent with greater *active* myocardial stiffness following SERCA down-regulation, complex alterations in passive stiffness and ventricular geometry may additionally contribute to local slowing of re-lengthening.

Beyond diastolic dysfunction, decreased SERCA expression has often been linked to declining systolic performance in HFrEF, particularly in humans and large animal models, where SERCA loss is associated with reduced SR Ca^{2+} content and release.[23] Presently, however, we observed that the reduction in SERCA activity was not accompanied by any reduction in SR Ca^{2+} load (*Figure 3B*), Ca^{2+} transient magnitude (*Figure 2B*), or fractional SR Ca^{2+} release (Supplementary material online, *Figure S2*). This is in line with previous results in small rodents, showing that Ca^{2+} transient magnitude is less markedly affected by SERCA reduction during heart failure, since action potential prolongation in these species augments triggering of Ca^{2+} release by L-type Ca^{2+} current.[29] In addition, the pronounced rise in diastolic Ca^{2+} observed at high pacing frequencies in the adjacent HFrEF region makes more Ca^{2+} available for SR reuptake, and thus release. Indeed, mathematical modelling revealed that transients simulated at 6 Hz with a 25% reduction in SERCA activity, only exhibited a modest reduction Ca^{2+} transient amplitude (*Figure 3F*). Conversely, in the remote region, the tendency towards higher NCX activity makes less Ca^{2+} available for SR reuptake, resulting in reduced SR Ca^{2+} content and smaller Ca^{2+} transients. Thus, while augmented NCX activity has compensatory effects on diastolic Ca^{2+} handling, such actions come at the expense of systolic Ca^{2+} release. The interplay between systolic and diastolic Ca^{2+} handling is also complicated by the fact that Ca^{2+} release and removal fluxes in fact overlap near the peak of the Ca^{2+} transient. We have previously shown that Ca^{2+} release is slowed and dyssynchronous in the adjacent region,[3] which is expected to delay and desynchronize the early phase of Ca^{2+} transient decline. However, due to the short time span of Ca^{2+} release compared with removal, we expect that such effects would be minor at late stages of the Ca^{2+} transient where we have estimated Ca^{2+} fluxes.

Other detrimental consequences of SERCA loss to be considered include increased susceptibility to pro-arrhythmic Ca^{2+} waves, impaired mechanoenergetics, and triggering of hypertrophy, SR/ER stress, and apoptotic signalling pathways.[23] As both remodelling and arrhythmogenesis are particularly pronounced in regions adjacent to an infarction,[30] a local reduction in SERCA expression can be speculated to locally contribute to these processes.

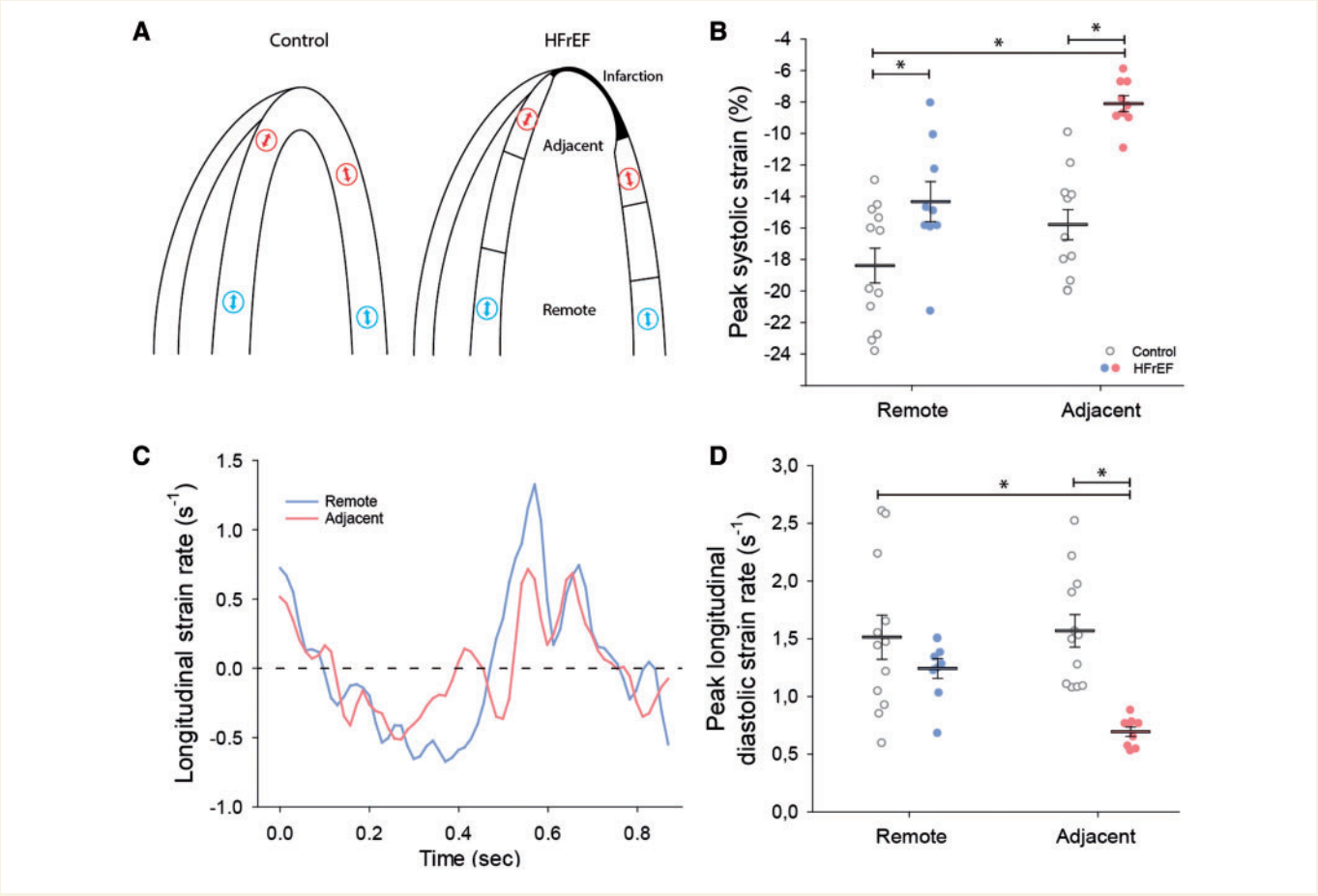

Figure 7 HFrEF patients exhibited regional diastolic dysfunction adjacent to the infarction. Four-chamber, apical echocardiographic images of HFrEF patients were examined to divide the viable myocardium into regions adjacent and remote to the myocardial infarction (schematically illustrated in *A*, right panel). Using speckle-tracking to examine local strain at indicated regions (arrows), comparison was made with regionally matched values in control hearts (*A*, left panel). Peak strain was reduced in HFrEF hearts, particularly in the adjacent region (*B*). Representative recordings of strain rate (*C*) and mean measurements (*D*) reveal that diastolic strain rate was also reduced adjacent to the myocardial infarction in HFrEF, but similar to control values in the remote region (n_{hearts} = 12, 9 in control, HFrEF). *$P < 0.05$ with two-way ANOVA with a *post hoc* Bonferroni *t*-test.

4.3 Role of elevated wall stress

What drives local remodelling adjacent to a myocardial infarction? Paracrine factors and neurohumoral activation likely play important roles. However, another potent trigger of remodelling—ventricular load—is also strikingly altered in the adjacent region, as tapering of the myocardium and curvature flattening toward the infarction result in locally high wall stress.[3,31] We recently demonstrated that elevated wall stress triggers disorganization of cardiomyocyte t-tubule structure, leading to slowed, de-synchronized Ca^{2+} release[3]; changes which are linked to reduced contractility in the adjacent region (*Figure 1B and C*). We presently demonstrate that heightened wall stress also down-regulates SERCA, further supporting the paradigm that excessive mechanical load plays a central role in disrupting myocardial structure and function during HFrEF. Intriguingly, in concentric hypertrophy, which acts to relieve wall stress, we recently observed that SERCA activity was enhanced and diastolic Ca^{2+} homoeostasis compensated.[14] Diastolic dysfunction in these hearts instead resulted from enhanced passive stiffness. In apparent agreement with wall-stress regulated expression of SERCA, it was previously observed that the expression of SERCA in dyssynchronous heart failure was down-regulated in the late-activated lateral wall which is subjected to excessive strain and stress,[32] whereas unloading of the heart by cardiac resynchronization therapy has been shown to restore SERCA expression.[33] Unloading of the failing heart by left ventricular assist devices also induces reverse remodelling, and in some cases up-regulation of SERCA,[34] providing further support for this paradigm. Thus, while it was previously recognized that high wall stress, particularly in the form of late systolic afterload, acutely slows relaxation,[35] our data indicate that heightened stress also has chronic effects on myocardial relaxation through remodelling of diastolic Ca^{2+} homoeostasis. In an effort to identify mechanosensitive signalling pathways which may trigger SERCA down-regulation, we investigated previously proposed regulators of SERCA expression, namely the ERK/MEK-pathway,[36] mir25,[37] and TNFα signalling.[38] While components of all three pathways tended to be up-regulated compared with sham, there was no evidence for marked specific up-regulation in the adjacent region compared with the more remote regions (Supplementary material online, *Figure S3*). Thus, although

the mechanosensitive mechanism leading to local SERCA loss remains unclear, an intriguing possibility is that locally distinct Ca^{2+} regulation adjacent to the infarction may contribute to such signalling.

5. Conclusion

In conclusion, we have demonstrated that regional variation in relaxation is associated with diastolic dysfunction in post-infarction HFrEF. Our data indicate that slowing of relaxation adjacent to the infarction is caused by elevated local wall stress, which triggers down-regulation of SERCA expression and slower diastolic Ca^{2+} removal. These findings establish a new paradigm implicating mechanical stress and cardiomyocyte Ca^{2+} homoeostasis as local determinants of diastolic function in health and disease.

Supplementary material

Supplementary material is available at *Cardiovascular Research* online.

Acknowledgements

The authors thank the Section of Comparative Medicine, Oslo University Hospital Ullevål (Oslo, Norway) for animal care, and the technical staff at the Institute for Experimental Medical Research for assistance with Western blotting and PCR assays.

Conflict of interest: none declared.

Funding

This work was supported by the European Union's Horizon 2020 research and innovation programme (Consolidator grant, WEL) under grant agreement No 647714. Additional support was provided by European Union Project No. FP7-HEALTH-2010.2.4.2-4 ('MEDIA-Metabolic Road to Diastolic Heart Failure'), The South-Eastern Norway Regional Health Authority, Anders Jahre's Fund for the Promotion of Science, The Norwegian Institute of Public Health, Oslo University Hospital Ullevål, and the University of Oslo.

References

1. Ponikowski P, Voors AA, Anker SD, Bueno H, Cleland JG, Coats AJ, Falk V, Gonzalez-Juanatey JR, Harjola VP, Jankowska EA, Jessup M, Linde C, Nihoyannopoulos P, Parissis JT, Pieske B, Riley JP, Rosano GM, Ruilope LM, Ruschitzka F, Rutten FH, van der Meer P; Authors/Task Force Members. 2016 ESC guidelines for the diagnosis and treatment of acute and chronic heart failure. *Eur Heart J* 2016;**37**:2129–2200.
2. Kramer CM, Lima JA, Reichek N, Ferrari VA, Llaneras MR, Palmon LC, Yeh IT, Tallant B, Axel L. Regional differences in function within noninfarcted myocardium during left ventricular remodeling. *Circulation* 1993;**88**:1279–1288.
3. Frisk M, Ruud M, Espe EK, Aronsen JM, Roe AT, Zhang L, Norseng PA, Sejersted OM, Christensen GA, Sjaastad I, Louch WE. Elevated ventricular wall stress disrupts cardiomyocyte t-tubule structure and calcium homeostasis. *Cardiovasc Res* 2016;**112**:443–451.
4. Bursi F, Weston SA, Redfield MM, Jacobsen SJ, Pakhomov S, Nkomo VT, Meverden RA, Roger VL. Systolic and diastolic heart failure in the community. *JAMA* 2006;**296**:2209–2216.
5. Brucks S, Little WC, Chao T, Kitzman DW, Wesley-Farrington D, Gandhi S, Shihabi ZK. Contribution of left ventricular diastolic dysfunction to heart failure regardless of ejection fraction. *Am J Cardiol* 2005;**95**:603–606.
6. Whalley GA, Gamble GD, Doughty RN. The prognostic significance of restrictive diastolic filling associated with heart failure: a meta-analysis. *Int J Cardiol* 2007;**116**:70–77.
7. Hasenfuss G, Schillinger W, Lehnart SE, Preuss M, Pieske B, Maier LS, Prestle J, Minami K, Just H. Relationship between Na^+-Ca^{2+}-exchanger protein levels and diastolic function of failing human myocardium. *Circulation* 1999;**99**:641–648.
8. Schmidt U, Hajjar RJ, Helm PA, Kim CS, Doye AA, Gwathmey JK. Contribution of abnormal sarcoplasmic reticulum ATPase activity to systolic and diastolic dysfunction in human heart failure. *J Mol Cell Cardiol* 1998;**30**:1929–1937.
9. Louch WE, Stokke MK, Sjaastad I, Christensen G, Sejersted OM. No rest for the weary: diastolic calcium homeostasis in the normal and failing myocardium. *Physiology (Bethesda)* 2012;**27**:308–323.
10. Sjaastad I, Sejersted OM, Ilebekk A, Bjornerheim R. Echocardiographic criteria for detection of postinfarction congestive heart failure in rats. *J Appl Physiol (1985)* 2000;**89**:1445–1454.
11. Espe EK, Aronsen JM, Skrbic B, Skulberg VM, Schneider JE, Sejersted OM, Zhang L, Sjaastad I. Improved MR phase-contrast velocimetry using a novel nine-point balanced motion-encoding scheme with increased robustness to eddy current effects. *Magn Reson Med* 2013;**69**:48–61.
12. Espe EKS, Skardal K, Aronsen JM, Zhang L, Sjaastad I. A semiautomatic method for rapid segmentation of velocity-encoded myocardial magnetic resonance imaging data. *Magn Reson Med* 2017;**78**:1199–1207.
13. Espe EK, Aronsen JM, Skardal K, Schneider JE, Zhang L, Sjaastad I. Novel insight into the detailed myocardial motion and deformation of the rodent heart using high-resolution phase contrast cardiovascular magnetic resonance. *J Cardiovasc Magn Reson* 2013;**15**:82.
14. Roe AT, Aronsen JM, Skardal K, Hamdani N, Linke WA, Danielsen HE, Sejersted OM, Sjaastad I, Louch WE. Increased passive stiffness promotes diastolic dysfunction despite improved Ca^{2+} handling during left ventricular concentric hypertrophy. *Cardiovasc Res* 2017;**113**:1161–1172.
15. Cheng H, Lederer WJ, Cannell MB. Calcium sparks: elementary events underlying excitation-contraction coupling in heart muscle. *Science* 1993;**262**:740–744.
16. Andersson KB, Birkeland JA, Finsen AV, Louch WE, Sjaastad I, Wang Y, Chen J, Molkentin JD, Chien KR, Sejersted OM, Christensen G. Moderate heart dysfunction in mice with inducible cardiomyocyte-specific excision of the Serca2 gene. *J Mol Cell Cardiol* 2009;**47**:180–187.
17. Gattoni S, Roe AT, Frisk M, Louch WE, Niederer SA, Smith NP. The calcium-frequency response in the rat ventricular myocyte: an experimental and modelling study. *J Physiol (Lond)* 2016;**594**:4193–4224.
18. Husebye T, Eritsland J, Muller C, Sandvik L, Arnesen H, Seljeflot I, Mangschau A, Bjornerheim R, Andersen GO. Levosimendan in acute heart failure following primary percutaneous coronary intervention-treated acute ST-elevation myocardial infarction. Results from the LEAF trial: a randomized, placebo-controlled study. *Eur J Heart Fail* 2013;**15**:565–572.
19. Husebye T, Eritsland J, Bjornerheim R, Andersen GO. Systolic mitral annulus velocity is a sensitive index for changes in left ventricular systolic function during inotropic therapy in patients with acute heart failure. *Eur Heart J Acute Cardiovasc Care* 2017;**7**:321–329.
20. Opdahl A, Remme EW, Helle-Valle T, Lyseggen E, Vartdal T, Pettersen E, Edvardsen T, Smiseth OA. Determinants of left ventricular early-diastolic lengthening velocity: independent contributions from left ventricular relaxation, restoring forces, and lengthening load. *Circulation* 2009;**119**:2578–2586.
21. Urheim S, Edvardsen T, Steine K, Skulstad H, Lyseggen E, Rodevand O, Smiseth OA. Postsystolic shortening of ischemic myocardium: a mechanism of abnormal intraventricular filling. *Am J Physiol Heart Circ Physiol* 2003;**284**:H2343–H2350.
22. Louch WE, Hougen K, Mork HK, Swift F, Aronsen JM, Sjaastad I, Reims HM, Roald B, Andersson KB, Christensen G, Sejersted OM. Sodium accumulation promotes diastolic dysfunction in end-stage heart failure following Serca2 knockout. *J Physiol (Lond)* 2010;**588**:465–478.
23. Roe AT, Frisk M, Louch WE. Targeting cardiomyocyte Ca^{2+} homeostasis in heart failure. *Curr Pharm Des* 2015;**21**:431–448.
24. Shattock MJ, Ottolia M, Bers DM, Blaustein MP, Boguslavskyi A, Bossuyt J, Bridge JH, Chen-Izu Y, Clancy CE, Edwards A, Goldhaber J, Kaplan J, Lingrel JB, Pavlovic D, Philipson K, Sipido KR, Xie ZJ. Na^+/Ca^{2+} exchange and Na^+/K^+-ATPase in the heart. *J Physiol (Lond)* 2015;**593**:1361–1382.
25. Pinali C, Bennett H, Davenport JB, Trafford AW, Kitmitto A. Three-dimensional reconstruction of cardiac sarcoplasmic reticulum reveals a continuous network linking transverse-tubules: this organization is perturbed in heart failure. *Circ Res* 2013;**113**:1219–1230.
26. Van Rooij E, Sutherland LB, Thatcher JE, DiMaio JM, Naseem RH, Marshall WS, Hill JA, Olson EN. Dysregulation of microRNAs after myocardial infarction reveals a role of miR-29 in cardiac fibrosis. *Proc Natl Acad Sci U S A* 2008;**105**:13027–13032.
27. Nagaraju CK, Dries E, Popovic N, Singh AA, Haemers P, Roderick HL, Claus P, Sipido KR, Driesen RB. Global fibroblast activation throughout the left ventricle but localized fibrosis after myocardial infarction. *Sci Rep* 2017;**7**:10801.
28. Urheim S, Edvardsen T, Torp H, Angelsen B, Smiseth OA. Myocardial strain by Doppler echocardiography. Validation of a new method to quantify regional myocardial function. *Circulation* 2000;**102**:1158–1164.
29. Louch WE, Hake J, Jolle GF, Mork HK, Sjaastad I, Lines GT, Sejersted OM. Control of Ca^{2+} release by action potential configuration in normal and failing murine cardiomyocytes. *Biophys J* 2010;**99**:1377–1386.
30. Stevenson WG, Soejima K. Catheter ablation for ventricular tachycardia. *Circulation* 2007;**115**:2750–2760.
31. Mitchell GF, Lamas GA, Vaughan DE, Pfeffer MA. Left ventricular remodeling in the year after first anterior myocardial infarction: a quantitative analysis of

contractile segment lengths and ventricular shape. *J Am Coll Cardiol* 1992;**19**: 1136–1144.
32. Spragg DD, Leclercq C, Loghmani M, Faris OP, Tunin RS, DiSilvestre D, McVeigh ER, Tomaselli GF, Kass DA. Regional alterations in protein expression in the dyssynchronous failing heart. *Circulation* 2003;**108**:929–932.
33. Vanderheyden M, Mullens W, Delrue L, Goethals M, de Bruyne B, Wijns W, Geelen P, Verstreken S, Wellens F, Bartunek J. Myocardial gene expression in heart failure patients treated with cardiac resynchronization therapy responders versus nonresponders. *J Am Coll Cardiol* 2008;**51**:129–136.
34. Heerdt PM, Holmes JW, Cai B, Barbone A, Madigan JD, Reiken S, Lee DL, Oz MC, Marks AR, Burkhoff D. Chronic unloading by left ventricular assist device reverses contractile dysfunction and alters gene expression in end-stage heart failure. *Circulation* 2000;**102**:2713–2719.
35. Brutsaert DL, de Clerck NM, Goethals MA, Housmans PR. Relaxation of ventricular cardiac muscle. *J Physiol (Lond)* 1978;**283**:469–480.
36. Huang H, Joseph LC, Gurin MI, Thorp EB, Morrow JP. Extracellular signal-regulated kinase activation during cardiac hypertrophy reduces sarcoplasmic/endoplasmic reticulum calcium ATPase 2 (SERCA2) transcription. *J Mol Cell Cardiol* 2014; **75**:58–63.
37. Wahlquist C, Jeong D, Rojas-Munoz A, Kho C, Lee A, Mitsuyama S, van Mil A, Park WJ, Sluijter JP, Doevendans PA, Hajjar RJ, Mercola M. Inhibition of miR-25 improves cardiac contractility in the failing heart. *Nature* 2014;**508**:531–535.
38. Tsai CT, Wu CK, Lee JK, Chang SN, Kuo YM, Wang YC, Lai LP, Chiang FT, Hwang JJ, Lin JL. TNF-alpha down-regulates sarcoplasmic reticulum Ca^{2+} ATPase expression and leads to left ventricular diastolic dysfunction through binding of NF-kappaB to promoter response element. *Cardiovasc Res* 2015;**105**:318–329.